Cluster spin-glass-like behavior in heavy-fermion-filled cage $Ce_3Co_4Sn_{13}$ doped with Fe: Magnetic and Mössbauer effect studies

L. Kalinowski, M. Kądziołka-Gaweł, and A. Ślebarski*

Institute of Physics, University of Silesia in Katowice, ul. 75 Pułku Piechoty 1, 41-500 Chorzów, Poland

(Received 31 October 2018; revised manuscript received 4 December 2018; published 26 December 2018)

We have measured the electric transport, magnetic properties, electronic structure, and ^{119}Sn Mössbauer spectra of a series of skutterudite-related $Ce_3Co_{4-x}Fe_xSn_{13}$ compounds, where x varies from 0 to 0.5. On the basis of these comprehensive studies, we report an observation of the spin-glass phase for samples with $x > 0.1$ Fe doping. The effect is, however, not observed for Ni dopants. The critical concentration close to $x = 0.1$ separates the magnetically ordered phase with $x > 0.1$ from the dense Kondo lattice phase ($x \leqslant 0.1$) with weak magnetic correlations. The Mössbauer spectra consist of three quadrupole doublets, related to covalent bonding among Sn2 and Ce as well as between Sn2 and Co/Fe atoms, which could be a reason for the structural deformation of the cages. These results confirm earlier structural investigations and are in agreement with the band-structure calculations, both of which indicated strong covalent bonding between the atoms M, Sn1, or Ce in the center of the cages and the Sn2 atoms forming the respective cages.

DOI: 10.1103/PhysRevB.98.245140

I. INTRODUCTION

The field skutterudite-like compounds of formula $Ce_3M_4Sn_{13}$, where M is a *d electron-type metal*, have been a group of strongly correlated electron systems (SCESs) attracting a great deal of attention for the past decade because of their unique low-temperature characteristics [1–5] resulting either from f- or d-electron correlations [6], as well as for their promising thermoelectric properties [7]. Systematic studies of these heavy fermions allowed us to observe new behaviors resulting from the subtle interplay between the crystal electric-field effect, magnetic interactions, and Kondo interactions. For example, we refer to our previous results [8], which showed in the specific-heat data of $Ce_3M_4Sn_{13}$ a field-induced crossover between a magnetically correlated Kondo-lattice state and a Kondo impurity phase. This field-induced phase transition is characteristic of SCESs with comparable Kondo and magnetic energy scales, and it suggests that $Ce_3M_4Sn_{13}$ could be near a magnetic quantum critical point (QCP). In such a critical regime, each perturbation (e.g., magnetic field or atomic disorder), regardless of how weak it may be, can have a significant effect by changing the nature of the quantum macrostate, and this enables us to observe novel phenomena. A transformation from a periodic crystal lattice to a more alloy-based system via an effective increase in disorder due to doping could lead to the magnetic ground state, as was reported for $CoSb_3$ skutterudite when the parent compound was doped with Fe [9,10]. This is, however, not the case for *nonmagnetic* $Ce_3Co_4Sn_{13}$ [11] when Ce is partially replaced by La [12] or Co by Ru [13]. In this paper, Co atoms in $Ce_3Co_4Sn_{13}$ are replaced in part by Fe, and the choice of Fe dopant is justified as follows. Most of the known iron-filled skutterudites are magnetic or weakly ferromagnetic metals (e.g., the family of MFe_4Sb_{12}, with M = Na,K,Ca,Sr,Ba,La,Yb [14]). $LaFe_4Sb_{12}$ is an enhanced Pauli paramagnet close to a ferromagnetic QCP with a spin fluctuation temperature ∼50 K, while $LaFe_4As_{12}$ exhibits ferromagnetism [15]. These observations suggest that in $Ce_3Co_4Sn_{13}$, Fe doping will also induce the magnetic ground state above a critical concentration of the dopant. The aim of the present work is to evaluate the ground-state properties of $Ce_3Co_4Sn_{13}$ doped with Fe to explore its impact on weak magnetic correlations between Ce atoms.

The high thermoelectric figure of merit observed for a field skutterudite compound 1 : 4 : 12 [16] results from a combination of a high Seebeck coefficient [17] and a *rattling* motion [18] leading to low thermal conductivity [19]. Good thermoelectric properties were also expected for $Ce_3M_4Sn_{13}$ skutterudite-related compounds due to the existence of similar Sn2 structural cages filled with Sn1, Ce, and M atoms, respectively. In recent reports, we documented [13] that strong covalent bonding excludes the rattling effect in the cages, but it could be a reason for structural instabilities observed for several $Ce_3M_4Sn_{13}$ and $La_3M_4Sn_{13}$ compounds. It was claimed that the cubic crystallographic structure $Pm\bar{3}n$ is modulated below temperature $T^\star$ [20]. The temperature $T^\star$ is spread over a wide range, from 350 K for $Ce_3Rh_4Sn_{13}$ [21,22], 311 K for $La_3Rh_4Sn_{13}$ [20], and 160 K for $Ce_3Co_4Sn_{13}$ [23] down to 150 K for $La_3Co_4Sn_{13}$ [23]. The structural second-order-type transition at $T^\star$ converts the simple-cubic high-temperature structure $Pm\bar{3}n$ into a body-centered-cubic structure $I4_132$ [24] due to the distortion of the $Sn1(Sn2)_{12}$ icosahedra related to a charge transfer from Sn2 toward Sn1 (see [5]). In [20] we argued that static atomic displacement of the atoms in the cages (treated as a kind of disorder) leads to a structural transition. Mössbauer spectroscopy makes this study possible. The advantage of ^{119}Sn Mössbauer spectroscopy is that it enables

*andrzej.slebarski@us.edu.pl

 ©2018 American Physical Society

us to examine directly the changes in the local environment and oxidation state of tin building the cages.

II. EXPERIMENTAL DETAILS

The samples were prepared using an arc-melting technique. Spectral pure elements at an appropriate mass ratio were remelted several times on a water-cooled cooper hearth in a high-purity argon atmosphere with an Al getter to ensure homogeneity and purity, and then annealed at 870 °C for two weeks. The obtained samples were examined by x-ray diffraction (XRD) analysis and found to have a cubic structure (space group $Pm\bar{3}n$) [25].

The XPS spectra were obtained at room temperature using a PHI 5700 ESCA spectrometer with monochromatized Al $K\alpha$ radiation.

Electrical resistivity ρ at ambient pressure was investigated by a conventional four-point ac technique using a PPMS (physical properties measurement system) device.

Magnetic ac susceptibility measurements were carried out using the PPMS platform. The dc magnetic susceptibility and magnetization were measured in the temperature range 1.8–400 K and in applied magnetic fields up to 7 T using a Quantum Design superconducting quantum interference device (SQUID) magnetometer.

The ^{119}Sn Mössbauer spectra were registered in the transmission geometry at room temperature by using a ^{119}Sn source in a $Ca^{119m}SnO_3$ matrix (15 mCi). The 23.875 keV γ-rays were detected using a proportional counter LND 45431. A palladium foil of 0.05 mm thickness was used to reduce the tin K x-rays concurrently emitted by this source. The velocity scale was calibrated by taking spectra of α-Fe. This calibration method is a standard one due to the narrowest and most well-defined spectral lines that the ^{57}Fe isotope possesses among all the known Mössbauer isotopes. Mössbauer absorbers were prepared in powder form. The ^{119}Sn isomer shifts are referenced to $BaSnO_3$, $\delta = 0.0$ mm/s. For the fitting of the experimental spectra, Lorentzian profiles and a least-squares method were used. The numerical analysis of the Mössbauer spectra was performed with the use of the WMOSS program [26].

III. RESULTS AND DISCUSSION

$Ce_3Co_4Sn_{13}$ is known as a paramagnetic heavy fermion dense Kondo system with a Kondo temperature $T_K \sim 1.5$ K [27]. The magnetic susceptibility and specific-heat analysis showed, however, the presence of weak short-range antiferromagnetic correlations in this system, which are not strong enough to promote long-range magnetic order [28] and are suppressed by an applied magnetic field. The field-induced phase transition between the magnetically correlated Kondo-lattice phase and a single-ion Kondo impurity state, very recently reported for $Ce_3Co_4Sn_{13}$ [8], suggested that the system can be near the quantum critical point (QCP). A similar crossover between these two states can also be caused by La doping near the critical concentration $x = x_c \sim 0.6$ in $Ce_{3-x}La_xCo_4Sn_{13}$ [12]. The question, therefore, is how the system will behave when Co is partially replaced by Fe ions. Will this doping lead to long-range magnetic order and QCP?

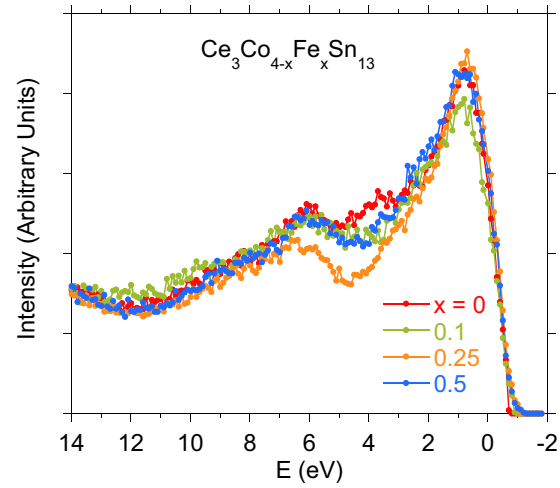

FIG. 1. Valence-band XPS spectra for the $Ce_3Co_{4-x}Fe_xSn_{13}$ samples ($x \leqslant 0.5$). The intensities of VBs are normalized to the same value at energy $E = 14$ eV.

Unfortunately, $Ce_3Fe_4Sn_{13}$ has not been obtained as a single phase; however, single-phase $Ce_3Co_{3-x}Fe_xSn_{13}$ compounds were identified for $x \leqslant 0.5$. Therefore, we investigated the components $x \leqslant 0.5$ of the series. Figure 1 shows valence-band (VB) XPS spectra of $Ce_3Co_{3-x}Fe_xSn_{13}$ with various x. The VB XPS spectra are very similar and dominated by Co/Fe $3d$ states [29]. Alloying does not noticeably modify the electronic bands [30–34]. The second broad maximum centered at ~6 eV is related to Sn $5s$ states, in agreement with recent band-structure calculations [13,29]. Here we are more focused on the effect of Fe doping of $Ce_3Co_4Sn_{13}$ on the electronic properties of Ce $4f$ bands located near the Fermi level ϵ_F. The effect of localization of the $4f$-electron states can be well described by the hybridization energy $V_{fc} \sim [\Delta/N(\epsilon_F)]^{1/2}$ between f and conduction (c) electron states within the framework of the Anderson model [35]. The energy Δ is of the order of energy of Kondo resonance, and it can be verified experimentally by Ce $3d$ and $4d$ core XPS spectra analysis (see Refs. [36,37] for the details of the method). Within the method [36], the hybridization energy Δ can be obtained from the ratio $I(f^2)/[I(f^1) + I(f^2)]$ of the respective $3d^9_{5/2}4f^n$ and $3d^9_{3/2}4f^n$ spin-orbit final states in Ce $3d$ XPS lines [see Fig. 2(b)]. Figure 2 shows the Ce $4d$ [Fig. 2(a)] and $3d$ [Fig. 2(b)] core-level XPS spectra. Based on the model, $\Delta \cong 130 \pm 25$ meV for $Ce_3Co_4Sn_{13}$, while Fe doping slightly decreases Δ to the value $\sim 100 \pm 20$ meV for sample $x = 0.5$. A small intensity of the $3d^94f^0$ final states suggests a stable configuration of Ce^{3+} ions in $Ce_3Co_{4-x}Fe_xSn_{13}$ [38]. Additional evidence for Ce^{3+} is shown in Fig. 2(a), namely the Ce $4d$ XPS spectra do not show satellite lines at the binding energies ~120 and 124 eV, characteristic of the mixed valence Ce-based systems [39,40]. On the basis of the above results, one can discuss the Ce $4f$ electron states in $Ce_3Co_{4-x}Fe_xSn_{13}$ as well-localized, and interpret a decrease of the hybridization energy Δ as an accompanying effect of Fe doping.

The χ versus T dc magnetic susceptibility data obtained at 500 Oe in a temperature range between 2 and 300 K in

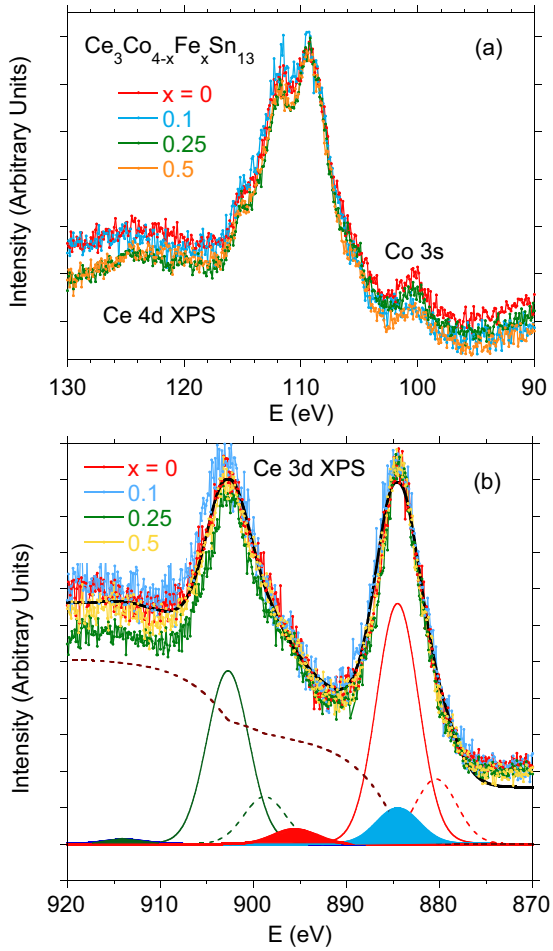

FIG. 2. Panel (a) shows the Ce $4d$ XPS spectra for $Ce_3Co_{4-x}Fe_xSn_{13}$ with no clear evidence of the $4d^9f^0$ final states at about 120 and 124 eV, characteristic of Ce-based mixed valence compounds. Panel (b) shows the Ce $3d$ XPS spectra for $Ce_3Co_{4-x}Fe_xSn_{13}$, and as an example, a deconvoluted spectrum for sample $x = 0.5$ on the basis of the Gunnarsson-Schönhammer theoretical model, with spin-orbit components $3d^9_{5/2}4f^n$ (red lines) and $3d^9_{3/2}4f^n$ (green lines), respectively, and $n = 1$ (solid lines), 2 (dashed lines), or 0 (fields). The brown dashed line represents the background, while the black line shows the fit after deconvolution to the XPS spectrum for sample $x = 0.5$. From the deconvolution procedure, the Sn $3s$ line contribution at 885 eV (blue field) provides about 15% of the total peak intensity due to $3d^9_{5/2}4f^1$ final states.

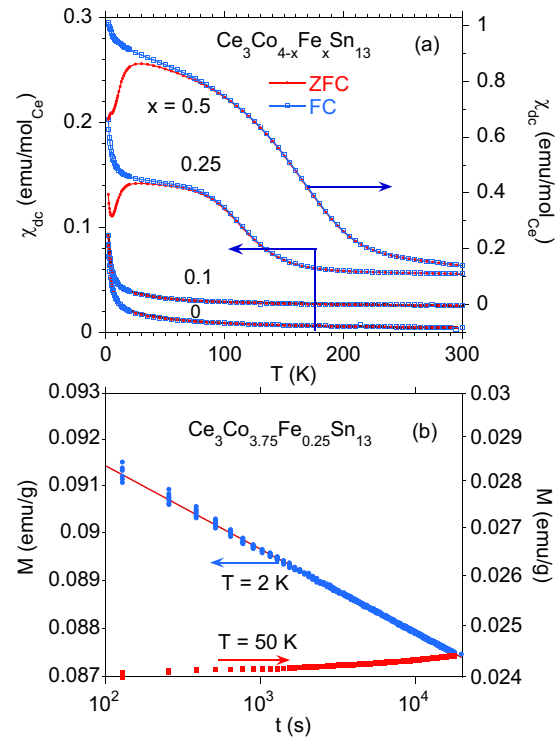

FIG. 3. Panel (a) shows ZFC and FC dc magnetic susceptibility for the series of $Ce_3Co_{4-x}Fe_xSn_{13}$ compounds in an external field of 500 Gs. The solid red line represents the CEF fit to $\chi(T)$ data (samples $x = 0$ and 0.1) for the two excited doublets separated from the ground-state doublet by energy Δ_1 and Δ_2, respectively. Panel (b) shows the time dependence of the isothermal remanent magnetization IRM for sample $x = 0.25$ measured at $T = 2$ K, i.e., below T_f and at 50 K (i.e., between T_f and T_d) in log-log scale. The solid line represents a least-squares fit using the expression $M(t) = M_0 t^{-\alpha}$.

zero-field-cooled (ZFC) and FC modes are shown in Fig. 3. The data of $Ce_3Co_4Sn_{13}$ and the sample $x = 0.1$ are well approximated by the Van Vleck formula [41] supplemented by the Pauli contribution χ_0,

$$\chi_{\mathrm{CEF}} = \frac{N_A\mu_B^2}{k_B}\frac{\sum_i\left(\frac{a_i}{T}+b_i\right)\exp\left(\frac{-\Delta_i}{k_BT}\right)}{\sum_i\exp\left(\frac{-\Delta_i}{k_BT}\right)} + \chi_0, \qquad (1)$$

considering the tetragonal Ce point symmetry ($J = 5/2$) with two doublets separated from the ground-state doublet by energies Δ_1 and Δ_2, respectively. Summations run over all i states of energies E_i, $\Delta_i = E_i - E_0$, N_A is the Avogadro number, and k_B is a Boltzmann constant. For $Ce_3Co_4Sn_{13}$, $\Delta_1 = 18.1$ K, $\Delta_2 = 69.7$ K, and $\chi_0 = 1.8 \times 10^{-3}$ emu/mol$_{\mathrm{Ce}}$, while for sample $x = 0.1$ the quantities $\Delta_1 = 45.7$ K, $\Delta_2 = 98.0$ K, and $\chi_0 = 2.0 \times 10^{-2}$ emu/mol$_{\mathrm{Ce}}$ are larger, respectively. The low-temperature $\chi \sim T^{-n}$ scaling with $n = 0.66$ or 0.45, observed for $Ce_3Co_4Sn_{13}$ and sample $x = 0.1$, respectively, in more than half of a decade could be related to the *disorder-induced non-Fermi-liquid* behavior [42]. Figure 3(a) shows for $Ce_3Co_{4-x}Fe_xSn_{13}$ with $x > 0.1$ burification in ZFC and FC χ curves below ~50 K characteristic of spin/cluster glasses, and above T_f strong deviation of $\chi(T)$ in CEF fit around 220 K. This type of deviation was first observed in Cu:Mn spin glasses, where cooperative correlations among the magnetic clusters have been observed at temperatures $T_d \approx 5T_f$. Figure 3(b) shows the isothermal remanent magnetization (IRM) as a function of time t, obtained at $T = 2$ and 50 K for the component $x = 0.25$. The sample was first zero-field-cooled from room temperature to 2 K, then a magnetic field of 1 T was applied for 5 min and switched off ($t = 0$). The observed time dependence of IRM at 2 K is characteristic of the canonical spin glasses and can be fitted by the power-law decay, $M(t) = M_0 t^{-\alpha}$, where $\alpha = 8.5 \times 10^{-3}$. Above temperature T_f the $M(t)$ behavior is quite different and does not show time relaxation of M.

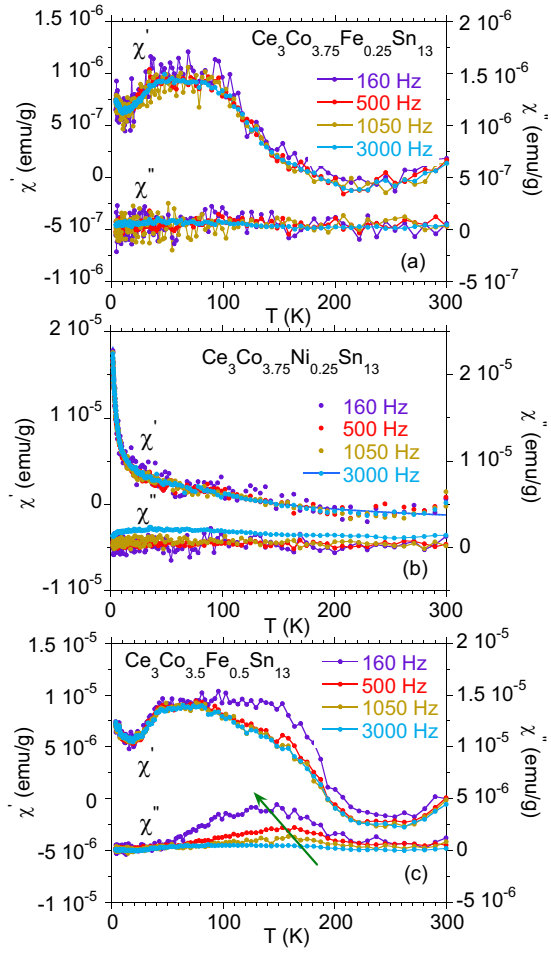

FIG. 4. The real and imaginary components of the ac magnetic susceptibility, χ' and χ'', for various frequencies as a function of temperature, measured for $Ce_3Co_{3.75}Fe_{0.25}Sn_{13}$ (a), reference compound $Ce_3Co_{3.75}Ni_{0.25}Sn_{13}$ (b), and for $Ce_3Co_{3.5}Fe_{0.5}Sn_{13}$ (c). In panel (b), the solid blue curve approximates the Van Vleck CEF expression [Eq. (1)] with energies $\Delta_1 = 11$ K and $\Delta_2 = 135$ K.

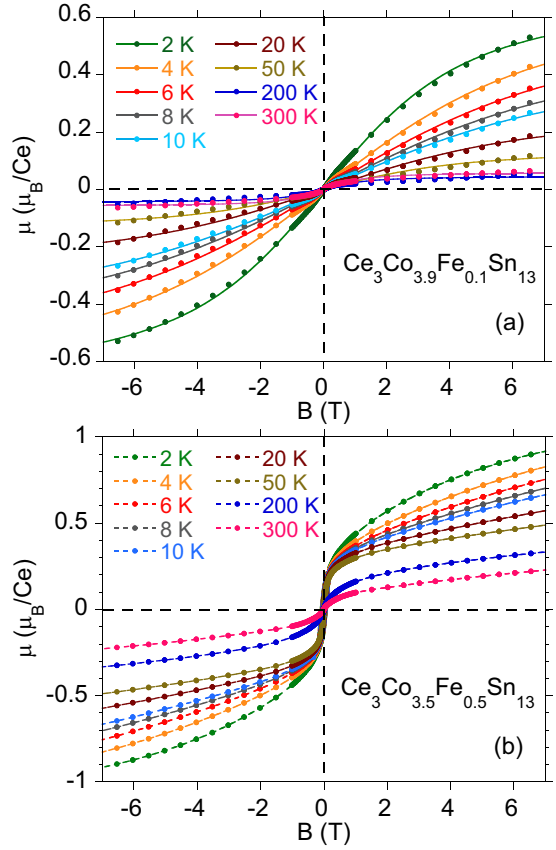

FIG. 5. Magnetization M vs magnetic field B for $Ce_3Co_{3.9}Fe_{0.1}Sn_{13}$ and the fit of the Langevin function (solid lines) to experimental data (a). Panel (b) shows $M(B)$ for $Ce_3Co_{3.5}Fe_{0.5}Sn_{13}$ at different temperatures; the data are not fitted by the Langevin function, and the M points are connected by a dashed line.

Figure 4 shows the ac susceptibility for the samples $x = 0.25$ [panel (a)] and $x = 0.5$ [panel (c)] at different frequencies with an amplitude 2 Oe of an applied ac field. The magnitude of component χ' shows a broad hump with a maximum at about T_f, while χ'' is weakly frequency (ν) -dependent. For comparison, we also present similar $\chi_{ac}(T)$ data for $Ce_3Co_4Sn_{13}$ doped with Ni ($x = 0.25$), which are typical of a paramagnet. The χ' is well approximated with the CEF expression [Eq. (1)], shown as a blue line with fitting parameters $\Delta_1 = 11$ K and $\Delta_2 = 135$ K, both of which are similar to that obtained for the parent $Ce_3Co_4Sn_{13}$ compound. The magnetization $M(B)$ isotherms are shown in Fig. 5. In panel (a) all isotherms of $Ce_3Co_{3.9}Fe_{0.1}Sn_{13}$ are well approximated by the Langevin function $L(\xi) = \coth(\xi) - 1/\xi$, where $\xi = \mu B/k_BT$, and μ is a total magnetic moment at T ($\mu = 0.72\mu_B$ is obtained for the isotherm at $T = 2$ K). A magnetization of $\sim 0.8\mu_B$/Ce is reached at 2 K for $Ce_3Co_4Sn_{13}$ and $Ce_3Co_{3.9}Fe_{0.1}Sn_{13}$ by extrapolation of M versus $1/B$ to $1/B \longrightarrow 0$. At 2 K the saturation magnetic moment increases to $\sim 1.1\,\mu_B$/Ce for sample $x = 0.5$, which signals the effect of magnetic Fe impurities.

The magnetization shows narrow hysteresis in the field dependence of M at $T < T_f$. Comprehensive magnetic results suggest that the doping of $Ce_3Co_4Sn_{13}$ with Fe atoms leads to spin-glass magnetic ordering if the concentration of Fe dopant $x > 0.1$. The magnetic ground state, however, was not observed for equivalent doping by Ni. It is very probable that in the series of $Ce_3Co_{3-x}Fe_xSn_{13}$ compounds, the critical concentration is slightly above concentration $x = 0.1$.

The ^{119}Sn Mössbauer spectra and transmission integral fits are shown for $Ce_3Co_{4-x}Fe_xSn_{13}$ in Fig. 6. The ^{119}Sn Mössbauer spectroscopy method (as a local probe technique) is very sensitive to the local atomic structure, its local deformation, and atomic or lattice defects such as vacancies or dislocations when treating the Sn nucleus as a probe of its local surrounding. For $Ce_3Co_{4-x}Fe_xSn_{13}$ compounds with the cubic symmetry $Pm\bar{3}n$ of the crystallographic structure, the Sn1 and Sn2 atoms occupy $2a$ and $24k$ Wyckoff positions, respectively, therefore one expects only two components in the ^{119}Sn Mössbauer spectra due to the occupation of these two different sites. However, a fitting procedure with only two components does not yield a good result, while three quadrupole split doublets well approximate the experimental

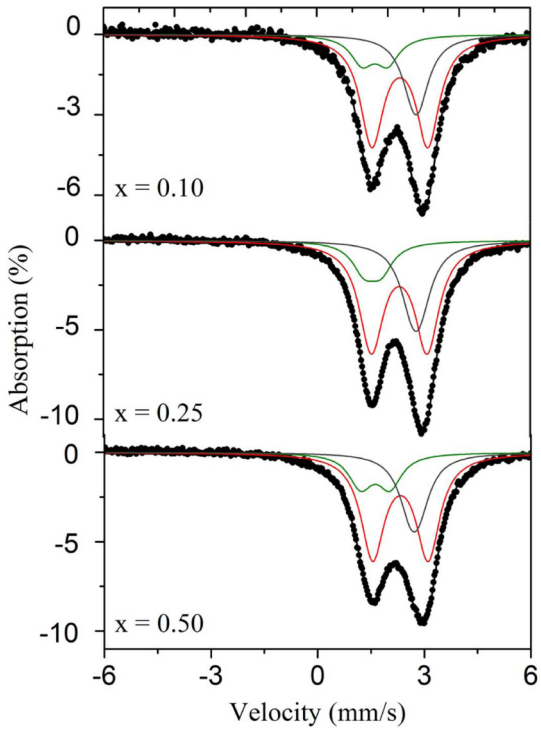

FIG. 6. The Mössbauer-effect spectra of several of the $Ce_3Co_{4-x}Fe_xSn_{13}$ compounds measured at room temperature.

data, as is shown in Fig. 6. Most of these components remain almost identical in three investigated $Ce_3Co_{4-x}Fe_xSn_{13}$ samples, which suggests that Sn atoms are located at the same crystal sites and are stable in there. One notes, however, that the presence of three doublets due to these different local surroundings of Sn atoms in the crystal structure of $Ce_3Co_{4-x}Fe_xSn_{13}$ indicates structural deviation from the symmetry $Pm\bar{3}n$ at $T = T^\star$ [43].

A summary of the Mössbauer spectral fitting parameters is given in Table I. Quadrupole doublet (1) with isomer shift $I_s = 2.70$ mm/s for sample $x = 0.1$ results from a tin

TABLE I. Mössbauer spectral parameters for $Ce_3Co_{4-x}Fe_xSn_{13}$ at room temperature: isomer shift I_s, electric quadrupole splitting Q_s, experimental full width at half-maximum G, and abundance of fitted component (A).

Component	I_s (mm/s)	Q_s (mm/s)	G (mm/s)	A (%)
		$Ce_3Co_{3.9}Fe_{0.1}Sn_{13}$		
doublet 1	2.70	0.16	0.80	24
doublet 2	1.54	0.78		15
doublet 3	2.24	1.57		61
		$Ce_3Co_{3.75}Fe_{0.25}Sn_{13}$		
doublet 1	2.70	0.22	0.82	27
doublet 2	1.47	0.47		15
doublet 3	2.22	1.57		58
		$Ce_3Co_{3.5}Fe_{0.5}Sn_{13}$		
doublet 1	2.69	0.23	0.81	27
doublet 2	1.53	0.82		17
doublet 3	2.23	1.56		56

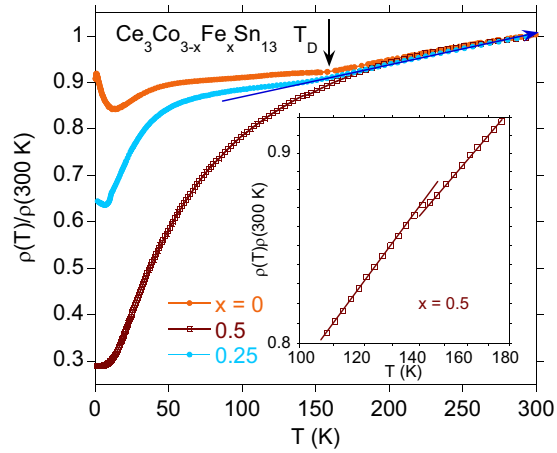

FIG. 7. Electrical resistivity $\rho(T)$ for $Ce_3Co_{4-x}Fe_xSn_{13}$, normalized by the resistivity at $T = 300$ K. The inset displays $\rho(T)$ near temperature T_D for sample $x = 0.5$ in log-log scale.

atom occupying the Sn1 position ($2a$ Wyckoff positions for space group $Pm\bar{3}n$). The value of I_s is not dependent on Fe doping and is ∼2.7 for the components $x = 0.1$, 0.25, and 0.5 of $Ce_3Co_{4-x}Fe_xSn_{13}$, and the electric quadrupole splitting stays essentially constant, which indicates that the electron bands are rigid, and no excitations of electrons to higher bands with different symmetry occur. The Sn1 ions are well trapped by Sn atoms in Sn2 positions, which agrees with recent band-structure calculations [5,6]. The Mössbauer spectra display two additional doublets (2 and 3) with different isomer shifts of about 1.51 and 2.23 mm/s (average value, see Table I), which indicates higher s-electron charge accumulation on one of the tin nuclei. These doublets are related to covalent bonding among Sn2 and Ce atoms as well as between Sn2 and Co/Fe, which could be a reason for the structural deformation of the cages. A similar behavior is also expected from recent band-structure calculations [5,6]. For doublet (2), both the average isomer shift of 1.57 mm/s and the quadrupole splitting value located in the range 0.47–0.82 mm/s are similar to those of rare-earth stannides [44]. The isomer shift of the third doublet is similar to that of the known intermetallic Sn-based compounds. Moreover, the cobalt atoms in the nearest environment of tin reduces in $Ce_3Co_4Sn_{13}$ the isomer shift in doublet (3) to the value of about 2.23 mm/s in respect to $I_s = 2.70$ mm/s of the doublet (1), the effect is attributed to charge transfer between the neighboring Sn and Co atoms (see Refs. [45–47] and [5]). In Table I the electric quadrupole interaction is found very similar for Fe and Co in $Ce_3Co_{3-x}Fe_xSn_{13}$ samples, which might be expected in view of the similarity both in their valence electron configuration and atomic environment.

Previous studies of $Ce_3Co_4Sn_{13}$ and similar isostructural compounds revealed [1] distinct anomalies in the electrical resistivity at $T_D \sim 160$ K with no structural signatures as a result of charge-density-wave (CDW) formation [48]. For most of the known $Ce_3M_4Sn_{13}$ compounds $T^\star > T_D$ [20,22], however, for $Ce_3Co_4Sn_{13}$ $T^\star$ [23] and T_D [1] are similar [43].

Figure 7 displays resistivity $\rho(T)$ for the series of $Ce_3Co_{4-x}Fe_xSn_{13}$ compounds. The absolute magnitude of the resistivity of $Ce_3Co_4Sn_{13}$ is ∼370 $\mu\Omega$ cm at room

temperature, similar value of ρ at $T = 300$ K was also obtained for the Fe-doped samples. This relatively high value of ρ is also characteristic of the series of other isostructural $Ce_3M_4Sn_{13}$ (and also $La_3M_4Sn_{13}$) compounds in the scattering processes of conduction electrons for several reasons: The involvement of strong correlation effect in the case of Ce-based samples [6], structural instability [49], nanoscale inhomogeneity [50], appearance of short-range correlations between atomic displacements [20], and other atomic defects of metallurgical nature. Resistivity ρ displays a metallic behavior above T_D, while below this temperature its behavior is typical of semimetals. Indeed, from *ab initio* calculations results, a pseudogap along the high-symmetry **k**-vector directions and a semimetallic character of $Ce_3Co_4Sn_{13}$ were predicted [5,29]. In the case of doping with Fe atoms, the d-electron states, more located at the Fermi level eliminate the pseudogap of $Ce_3Co_4Sn_{13}$, in result the resistance ratio significantly increases with Fe doping, as is shown in Fig. 7. The resistivity value has been normalized to that corresponding for $T = 300$ K to better compare the data. The appearance of CDW phase is clearly visible in ρ data at T_D, for sample $x = 0.5$ the effect is weak, as is shown in the inset to the figure.

The anomaly in $\rho(T)$ at T_D correlates with the observed displacement of Sn2 atoms obtained from the Mössbauer effect spectra.

IV. CONCLUDING REMARKS

We report a change in the magnetic properties of the skutterudite-related $Ce_3Co_4Sn_{13}$ Kondo system, which evolves from a Kondo lattice state with weak short-range magnetic correlations between Ce f-electron magnetic moments and the cluster spin-glass-like magnetic phase when the parent compound is doped by Fe. A critical concentration $x = x_c \gtrsim 0.1$ in the series of $Ce_3Co_{3-x}Fe_xSn_{13}$ compounds. A power law in $\chi \sim T^{-n}$ data for $Ce_3Co_4Sn_{13}$ and the sample $x = 0.1$ with exponent $n \sim 0.5$ is characteristic of Ce-based disordered systems close to quantum criticality at QCP, while the components x with Fe content larger than 0.1 exhibit in $\chi(T)$ and $M(B)$ data spin-glass-like behavior and time relaxation of isothermal remanent magnetization. When Ce is replaced in part by La or Co by Ni, the evolution to the ordered magnetic ground state has not been documented. It is worth noting that substitution of Co with Ru atoms does not cause such a magnetic evolution [13], although the Fe and Ru atoms are included in the same group of the Periodic Table. We also present the ^{119}Sn Mössbauer spectra at room temperature, which confirm experimentally a charge accumulation between Co/Fe and Sn atoms in the cage. A similar effect was reported earlier on the basis of DFT calculations. The covalent bonding due to charge accumulation between respective atoms eliminates the rattling effect in these types of materials; however, it is a reason for the structural transformation at $T^\star$ [20,22,23,51].

ACKNOWLEDGMENTS

L.K. and A.Ś. thank the National Science Centre (NCN) for financial support on the basis of Decission No. DEC-2014/15/N/ST3/03799. A.Ś. also thanks the Kosciuszko Foundation for the partial support of the research.

[1] E. L. Thomas, H.-O. Lee, A. N. Bonkston, S. MaQuilon, P. Klavins, M. Moldovan, D. P. Young, Z. Fisk, and J. Y. Chan, J. Solid State Chem. **179**, 1642 (2006).
[2] A. Ślebarski, B. D. White, M. Fijałkowski, J. Goraus, J. J. Hamlin, and M. B. Maple, Phys. Rev. B **86**, 205113 (2012).
[3] A. Ślebarski and J. Goraus, Phys. Rev. B **88**, 155122 (2013).
[4] A. Ślebarski, P. Witas, J. Goraus, L. Kalinowski, and M. Fijałkowski, Phys. Rev. B **90**, 075123 (2014).
[5] A. Ślebarski, J. Goraus, and P. Witas, Phys. Rev. B **92**, 155136 (2015).
[6] A. Ślebarski, J. Goraus, P. Witas, L. Kalinowski, and M. Fijałkowski, Phys. Rev. B **91**, 035101 (2015).
[7] U. Köhler, A. Pikul, N. Oeschler, T. Westerkamp, A. M. Strydom, and F. Steglich, J. Phys.: Condens. Matter **19**, 386207 (2007).
[8] A. Ślebarski and J. Goraus, Physica B **536**, 165 (2018).
[9] J. Yang, G. P. Meisner, D. T. Morelli, and C. Uher, Phys. Rev. B **63**, 014410 (2000).
[10] P. Amornpitoksuk, D. Ravot, A. Mauger, and J. C. Tedenac, J. Alloys. Compds. **440**, 295 (2007).
[11] In most of the known $Ce_3M_4Sn_{13}$ heavy fermions, the magnetic susceptibility and specific heat indicated the presence of weak short-range antiferromagnetic-type correlations, which are not strong enough to promote long-range magnetic order.
[12] A. Ślebarski, M. Fijałkowski, and J. Goraus, Intermetallics **54**, 199 (2014).
[13] L. Kalinowski, J. Goraus, P. Witas, and A. Ślebarski, Phys. Rev. B **94**, 235151 (2016).
[14] W. Schnelle, A. Leithe-Jasper, H. Rosner, R. Cardoso-Gil, R. Gumeniuk, D. Trots, J. A. Mydosh, and Yu. Grin, Phys. Rev. B **77**, 094421 (2008).
[15] S. Tatsuoka, H. Sato, K. Tanaka, M. Ueda, D. Kikuchi, H. Aoki, T. Ikeno, K. Kuwahara, Y. Aoki, H. Sugawara, and H. Harima, J. Phys. Soc. Jpn. **77**, 033701 (2008).
[16] B. C. Sales, D. Mandrus, and R. K. Williams, Science **272**, 1325 (1996).
[17] L. Nordström and D. J. Singh, Phys. Rev. B **53**, 1103 (1996).
[18] W. Jeitschko and D. Braun, Acta Crystallogr., Sect. B **33**, 3401 (1977).
[19] D. T. Morelli and G. P. Meisner, J. Appl. Phys. **77**, 3777 (1995).
[20] A. Ślebarski, P. Zajdel, M. Fijałkowski, M. M. Maśka, P. Witas, J. Goraus, Y. Fang, D. C. Arnold, and M. B. Maple, New J. Phys. **20**, 103020 (2018).
[21] C. N. Kuo, W. T. Chen, C. W. Tseng, C. J. Hsu, R. Y. Huang, F. C. Chou, Y. K. Kuo, and C. S. Lue, Phys. Rev. B **97**, 094101 (2018).
[22] K. Suyama, K. Iwasa, Y. Otomo, K. Tomiyasu, H. Sagayama, R. Sagayama, H. Nakao, R. Kumai, Y. Kitajima, F. Damay, J. M. Mignot, A. Yamada, T. D. Matsuda, and Y. Aoki, Phys. Rev. B **97**, 235138 (2018).

[23] Y. Otomo, K. Iwasa, K. Suyama, K. Tomiyasu, H. Sagayama, R. Sagayama, H. Nakao, R. Kumai, and Y. Murakami, Phys. Rev. B **94**, 075109 (2016).

[24] P. Bordet, D. E. Cox, G. P. Espinosa, J. L. Hodeau, and M. Marezio, Solid State Commun. **78**, 359 (1991).

[25] J. P. Remeika, G. P. Espinosa, A. S. Cooper, H. Barz, J. M. Rowel, D. B. McWhan, J. M. Vandenberg, D. E. Moncton, Z. Fizk, L. D. Woolf, H. C. Hamaker, M. B. Maple, G. Shirane, and W. Thomlinson, Solid State Commun. **34**, 923 (1980); J. L. Hodeau, M. Marezio, J. P. Remeika, and C. H. Chen, *ibid.* **42**, 97 (1982).

[26] I. Prisecaru, *WMOSS4 Mössbauer Spectral Analysis Software*, http://www.wmoss.org, 2009-2016.

[27] A. L. Cornelius, A. D. Christianson, J. L. Lawrence, V. Fritsch, E. D. Bauer, J. L. Sarrao, J. D. Thompson, and P. G. Pagliuso, Physica B **378-380**, 113 (2006).

[28] A. D. Christianson, E. A. Goremychkin, J. S. Gardner, H. J. Kang, J.-H. Chung, P. Manuel, J. D. Thompson, J. L. Sarrao, and J. L. Lawrence, Physica B **403**, 909 (2008).

[29] G. Zhong, X. Lei, and J. Mao, Phys. Rev. B **79**, 094424 (2009).

[30] Previous band-structure calculations for the known skutterudites of $CeFe_2X_{12}$ type (e.g., [31–33]) or metallic cubic Heusler alloys (e.g., [34]) showed that Fe d-electron bands are located between the Fermi energy and binding energy of about 4 eV. One therefore expects a similar location of the $3d$ bands of Co and Fe dopant in the valence bands of $Ce_3Co_{4-x}Fe_xSn_{13}$, and a strong hybridization effect between them.

[31] K. Nouneh, A. H. Reshak, S. Auluck, I. V. Kityk, R. Viennois, S. Benet, and S. Charar, J. Alloys. Compd. **437**, 39 (2007).

[32] R. Khenata, A. Bouhemadou, A. H. Reshak, R. Ahmed, B. Bouhafs, D. Rached, Y. Al-Douri, and M. Rérat, Phys. Rev. B **75**, 195131 (2007).

[33] M. Hachemaoui, R. Khenata, A. Bouhemadou, A. H. Reshak, D. Rached, and F. Semari, Curr. Opin. Solid State Mater. Sci. **13**, 105 (2009).

[34] A. Ślebarski, J. Phys. D **39**, 856 (2006).

[35] P. W. Anderson, Phys. Rev. **124**, 41 (1961).

[36] O. Gunnarsson and K. Schönhammer, Phys. Rev. B **28**, 4315 (1983); J. C. Fuggle, F. U. Hillebrecht, Z. Zolnierek, R. Lässer, Ch. Freiburg, O. Gunnarsson, and K. Schönhammer, *ibid.* **27**, 7330 (1983).

[37] A. Ślebarski, M. Radłowska, T. Zawada, M. B. Maple, A. Jezierski, and A. Zygmunt, Phys. Rev. B **66**, 104434 (2002); A. Ślebarski, T. Zawada, J. Spałek, and A. Jezierski, *ibid.* **70**, 235112 (2004).

[38] On the basis of the theoretical method of Gunnarsson and Schönhammer [36], the $4f$ shell occupation number $n_f = I(f^0)/[I(f^0) + I(f^1) + I(f^2)]$ is less than 0.04.

[39] A. J. Signorelli and R. G. Hayes, Phys. Rev. B **8**, 81 (1973).

[40] Y. Baer, R. Hauger, Ch. Zürcher, M. Campagna, and G. K. Wertheim, Phys. Rev. B **18**, 4433 (1978).

[41] J. Mulak, J. Less Common Met. **121**, 141 (1986).

[42] G. R. Stewart, Rev. Mod. Phys. **73**, 797 (2001).

[43] The *high-temperature* structural transition $T_{\rm HT}$ connected to atomic disorder subsequently leads to the long-range superstructure at $T^\star$ and the subtle effects observed at T_D, which leave no structural signatures, and $T_D < T^\star < T_{\rm HT}$ (for details, see [20]).

[44] T. Schmidt, D. Johrendt, C. P. Sebastian, R. Pöttgen, K. Łatka, and R. Kmieć, Naturforsch. B **60**, 1036 (2005).

[45] G. F. Ortiz, R. Alcántara, I. Rodriguez, and J. L. Tirado, J. Electroanal. Chem. **605**, 98 (2007).

[46] R. Alcántara, P. Lavela, G. Ortiz, I. Rodriguez, and J. L. Tirado, Hyperfine Interact. **187**, 13 (2008).

[47] A. Vertes, J. Jaén, and M. L. Varsanyi, J. Radioanal. Nucl. Chem. **90**, 383 (1985).

[48] C. S. Lue, H. F. Liu, S.-L. Hsu, M. W. Chu, H. Y. Liao, and Y. K. Kuo, Phys. Rev. B **85**, 205120 (2012); H. F. Liu, C. N. Kuo, C. S. Lue, K.-Z. Syu, and Y. K. Kuo, *ibid.* **88**, 115113 (2013).

[49] L. E. Klintberg, S. K. Goh, P. L. Alireza, P. J. Saines, D. A. Tompsett, P. W. Logg, J. Yang, B. Chen, K. Yoshimura, and F. M. Grosche, Phys. Rev. Lett. **109**, 237008 (2012).

[50] A. Ślebarski, M. Fijałkowski, M. M. Maśka, M. Mierzejewski, B. D. White, and M. B. Maple, Phys. Rev. B **89**, 125111 (2014).

[51] L. Mendonca-Ferreira, F. B. Carneiro, M. B. Fontes, E. Baggio-Saitovitch, L. S. I. Veiga, J. R. L. Mardegan, J. Strempfer, M. M. Piva, P. G. Pagliuso, R. D. dos Reis, and E. M. Bittar, J. Alloys. Compds. **773**, 34 (2019).